J. Appl. Comput. Mech., 8(2) (2022) 671-683
DOI: 10.22055/JACM.2021.38781.3312

ISSN: 2383-4536
jacm.scu.ac.ir

Shahid Chamran University of Ahvaz

Journal of Applied and Computational Mechanics

Research Paper

Impact-enhanced Electrostatic Vibration Energy Harvester

Valery P. Dragunov[1], Dmitriy I. Ostertak[1], Dmitry E. Kiselev[1], Evgeniya V. Dragunova[2]

[1] Department of Semiconductor Devices and Microelectronics, Novosibirsk State Technical University,
Karl Marx Avenue 20, Novosibirsk, 630073, Russia, Email: dragunov@corp.nstu.ru, ostertak@ngs.ru, dkiselev.nstu@gmail.com

[2] Department of Computer Science in Economics, Novosibirsk State Technical University, Karl Marx Avenue 20, Novosibirsk, 630073, Russia, Email: evdragunova@ngs.ru

Received October 20 2021; Revised December 1 2021; Accepted for publication December 11 2021.
Corresponding author: D.I. Ostertak (ostertak@ngs.ru)

Abstract. An influence of mechanical impacts between variable capacitor electrodes on the electrostatic vibration energy harvester (e-VEH) operation is studied theoretically. The analysis is carried out for two conditioning circuits with parallel and serial load connection. A relationship between e-VEH parameters and external mechanical force characteristics enabling to assess the possibility of operation in a periodic impact mode is obtained. Dependences of the average power generated by the impact-enhanced e-VEH versus the number of collisions between the electrodes and the load resistor value are calculated. The operation of the harvester for two circuits in impact and non-impact modes is compared and analyzed. It is shown that the average power generated by the e-VEH for the impact mode can exceed the power for the non-impact mode by 1–2 orders of magnitude along with a significant decrease of the harvester optimal load resistance.

Keywords: MEMS, vibration energy harvesting, periodicity, power, spatial limitations.

1. Introduction

Currently, both separately located sensors and entire wireless sensor networks (WSN) are widely used to monitor various physical parameters or the state of an object in real time. Such autonomous networks have the ability to self-organize and high fault tolerance, which define their application areas: monitoring of the environment and human health, security control, protection of remote facilities, etc [1, 2].

A WSN node requires a power source for operation, which should be autonomous and maintenance-free. Therefore, power sources based on the conversion of renewable energy into electrical one are very promising, such as solar radiation, wind force, ocean tide, thermal and vibration energy, etc [3, 4]. Mechanical vibrations are considered as the most convenient source in terms of the device size and suitability for many purposes [5-8]. There are a lot of mechanical vibration sources in environment: natural phenomena, industry, transport, operation of various machines, walking and other human activities, etc.

Thanks to development of microelectronics industry small-sized, low-power and reliable microelectromechanical systems (MEMS) have appeared that are widely used today in many fields of science, technology and human life [9, 10]. One of the most utilized types of MEMS devices is microelectromechanical converters (MEMC), which are designed to convert mechanical energy (or vibrations) into electrical one. There are three main types of MEMC: piezoelectric [11-13], electromagnetic [14-16] and electrostatic [17-19]. Electrostatic converters are the most promising due to their relatively easy fabrication and integration with CMOS technology, their operation is based on the capacitance modulation of a variable capacitor under the influence of external mechanical forces (or vibrations). The electrostatic MEMC along with an appropriate conditioning circuit represent the so-called electrostatic vibration energy harvester (e-VEH) [20-28].

The development and improvement of the MEMCs and e-VEHs based on them are primarily focused on increasing the average generated power, as well as reducing their weight and size parameters. In this connection spatial restrictions in the design of the devices appear that somehow affect their operation.

In order to increase the output power of the e-VEH, as a rule, they strive to increase the capacitance modulation depth of the variable capacitor $\eta = C_{max}/C_{min}$, and the charge q_0 taken from the primary power source V_0 by increasing its voltage (where C_{max} and C_{min} are the maximal and minimal values of the capacitance). However, when the MEMC dimensions decrease the both possibilities become significantly limited. Since if the interelectrode gap is decreased then the minimal capacitance of the variable capacitor C_{min} and the probability of electrical breakdown increase.

Theoretically, the MEMC power can also be increased by decreasing the duration of the energy conversion cycle and increasing the number of conversion cycles during the period of external mechanical vibrations [29-34]. It can be achieved by using additional forces arising in the system when the variable capacitor electrodes collide with each other. Such a new type of the MEMC with impacts seems to be very promising [29-31, 34-36]. However, the analysis of these MEMC is currently fragmentary, and their practical implementation is not yet available. Without a detailed analysis, taking into account a specific conditioning circuit of the harvester it is not clear at all whether an increase of the generated power will be achieved or not, because when the

Published online: December 18 2021

collision frequency increases the amplitude of the movable electrode rebound and the capacitance modulation depth decrease. Such a multifactorial system turns out to be very complex and for its analysis, especially at the stage of preliminary design, it is desirable to have analytical methods for analyzing the features of the system operation.

This work is devoted to modeling and comparative analysis of the e-VEH operation comprising two-electrode impact and non-impact MEMC.

2. MEMC Model

Prior to analysis of the e-VEH operation let's consider some features of its most important part, MEMC. Similarly to the classic (non-impact) MEMC the impact converter is also a variable capacitor. The schematic configuration of the two-electrode MEMC and its mechanical model used for simulation are shown in Fig. 1(a) and Fig. 1(b), respectively. The converter comprises the case walls rigidly connected to the middle part consisting from the movable electrode, spring elements and frame. One of the variable capacitor electrodes is located on the right wall of the case (RWC). The second electrode is on the movable part which can freely move between the left and right walls. Here the left wall of the case (LWC) is necessary to limit the motion of the movable mass. Also the stoppers were assumed to prevent the pull-in effect between the electrodes. There are also the stoppers on the LWC. It was assumed during the analysis that the maximal value of the gap between the stoppers on the RWC and the movable electrode is d_0. The height of the stoppers was chosen proportional to the interelectrode gap d_0 and was equal to μd_0, where μ is the coefficient of proportionality.

During the motion of the converter case according to the law y(t), which is determined by the external mechanical force, the movable electrode with mass of M_1 suspended on the spring elements with the total stiffness of k is involved to the oscillation process according to the law z(t). In this case, the movable electrode is suffered from the elastic forces tending to return it to the equilibrium position and also from the electrostatic force of attraction due to the applied voltage between the electrodes.

As a result the gap between the stoppers on the LWC and the movable electrode is varied according to x(t), where for linear approximation of the mechanical force the equilibrium equation can be represented as

$$M_1 \frac{d^2\delta}{dt^2} + B\frac{d\delta}{dt} + k\delta - F_e = -M_1 \frac{d^2y}{dt^2}, \tag{1}$$

where $\delta = d_0 - x$ is a current value of the gap between the stoppers on the RWC and the movable electrode, F_e is the electrostatic force, and B is the damping force coefficient.

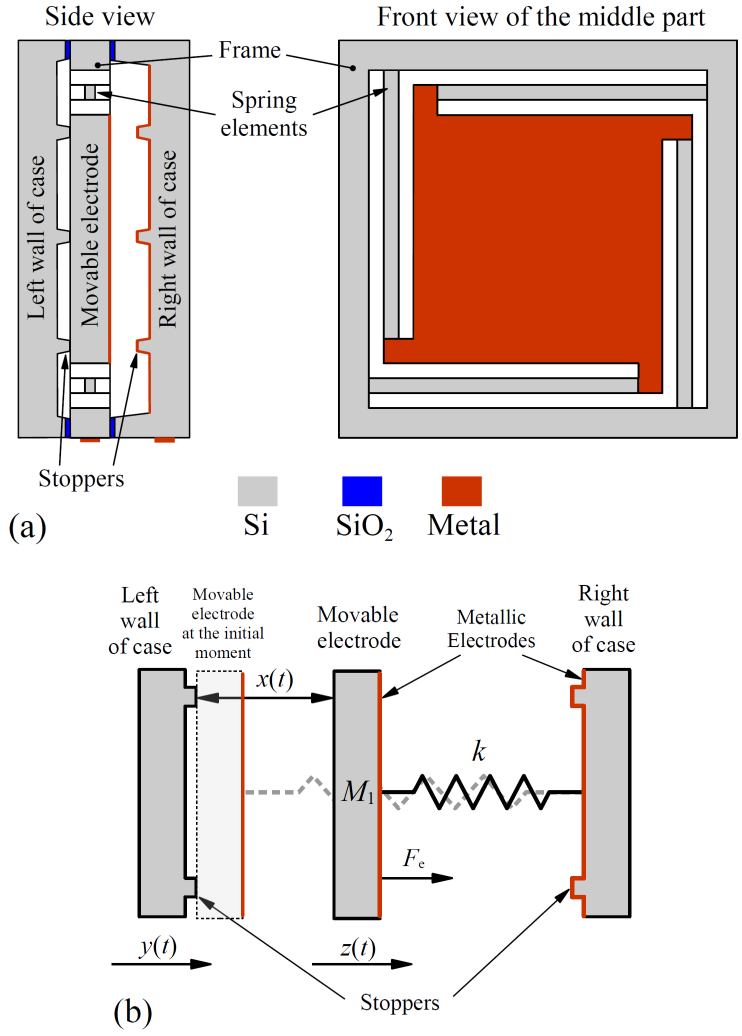

Fig. 1. The schematic configuration of the considered two-electrode electrostatic energy converter (a) and its mechanical model used for simulation (b).

Table 1. MEMC parameters used for calculation of the movable electrode displacement trajectory with a stochastic behavior.

Parameter	Symbol	Value
Maximal value of the gap	d_0	5.8 μm
Stoppers height	μd_0	0.1 μm
Stiffness coefficient	k	200 N/m
Damping force coefficient	B	0.01 kg/s
Movable electrode mass	m	0.39 g
Movable electrode area	S	5×5 mm²
External vibration frequency	$\omega / 2\pi$	36 Hz
Amplitude of the case oscillations	A_0	0.5 mm

Equation (1) describes the movable electrode motion only for intervals between the impacts against the stoppers. For taking into account the impacts at the moments of contact between the movable electrode and the stoppers the classic theory of impacts was used, where the speed of the colliding bodies after an impact is defined by

$$V_1 = v_1 + (1+e)\frac{M_2}{M_1+M_2}(v_2 - v_1),$$
$$V_2 = v_2 + (1+e)\frac{M_1}{M_1+M_2}(v_1 - v_2), \tag{2}$$

where M_2 is the case mass, e is the velocity recovery coefficient during the impact, v_1 and v_2 are velocities of the movable electrode and the case before the impact, respectively, and V_1 and V_2 the corresponding velocities after the impact. It was assumed that the mass of the case is much greater than the mass of the movable electrode, the impacts do not change motion characteristics of the case, and the value of e is equal to 1 corresponding to an absolutely elastic impact.

Let's analyze the motion features of the MEMC movable plate under the conditions of the absence of the electrical, damping and elastic forces. We will also assume that the movable electrode experiences collisions only with the RWC (the velocity v_1 at the moment of contact is not equal to v_2) and just only comes into a contact with the left wall, i.e. the velocity v_1 at the moment of touching the LWC is equal to v_2.

We will consider that at the initial moment of time $t_0 = -0.25T$ the movable electrode was in contact with the LWC, and the case itself was in the extreme left position (here T is the period of the case oscillation). At the beginning of the case motion to the right side the movable electrode pushed by the LWC will also begin to move in the same direction. If the case moves according to a harmonic motion with the law $y(t) = A_0\sin(\omega t)$, then their joint movement at the same speed will continue until the case speed reaches its maximal value of $v_2\,(t = 0) = A_0\omega$, where A_0 and ω are the amplitude and the angular frequency of the case oscillations. After that (when $t > 0$) the case motion will slow down, but the movable electrode will continue to move at the speed of $v_1\,(t = 0) = v_2\,(t = 0) = A_0\omega$. At the moment of time t_1 the movable electrode will catch up the stoppers on the RWC and their collision will occur, after that the case will continue to move with the speed of $V_2(t) = v_2(t) = A_0\omega\cos(\omega t)$, but the movable electrode will move with the speed of $V_1(t_1) = 2v_2(t_1) - v_1(t = 0)$. Afterwards the movable electrode at the moment of t_2 can again come into a contact with the RWC or the LWC.

Using the system of Equations (1) and (2) it is possible to calculate the time dependence of the gap between the stoppers on the RWC and the movable electrode for different parameters of MEMC. This gap under the assumption made can be given by

$$\delta = d_0 - \left(Y_0 + v_0 t + A_0\left[\omega t - \sin(\omega t)\right]\right),$$

where Y_0 and v_0 the initial displacement and velocity of the movable electrode calculated after each collision.

Numerical analysis shows that in general the displacement of the movable electrode relative to the case is non-periodic, i.e. the system behaves in a stochastic manner. An example of the calculated displacement trajectory of the movable electrode with a stochastic behavior for MEMC with parameters presented in Table 1 is shown in Fig. 2.

Considering this behavior of the movable electrode, even the average power developed by the microgenerator (e-VEH) can change over time. From this point of view, it is of interest to search for solutions where the motion of the movable electrode will be periodic.

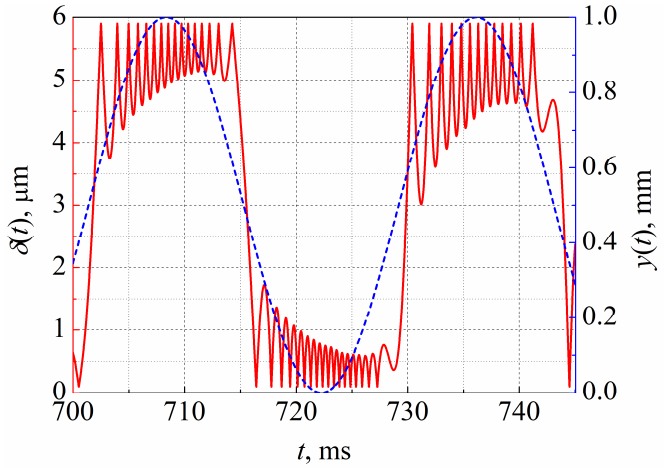

Fig. 2. The trajectory of the movable electrode displacement δ with a stochastic behavior (red line), and the MEMC case displacement (blue line).

In order for the behavior of the system to become periodic, when compiling a system of equations describing its motion, it is necessary to take into account that $v_1(t)$ and $V_1(t)$ should be equal to $v_1(t+T)$ and $V_1(t+T)$, respectively. In this case, e.g. for the MEMC with four collisions during the period of the case vibration, the system of corresponding equations that determines the MEMC parameters is defined as

$$\frac{d_0}{A_0} = \omega t_1 - \sin(\omega t_1),$$

$$\frac{d_0}{A_0} = \omega t_1 - \sin(\omega t_2) + \omega[2\cos(\omega t_1) - 1](t_2 - t_1), \tag{3}$$

$$2\cos(\omega t_2) - 2\cos(\omega t_1) + 1 = 0,$$

where t_1 and t_2 the time of the first and second impacts, respectively. In this case the time of the third impact t_3 will be equal to $0.5T - t_2$, and the fourth one is $t_4 = 0.5T - t_1$.

Under the assumptions made, periodic behavior will be possible only with a certain ratio between the amplitude A_0 of the case vibrations and the maximum gap d_0 between the stoppers on the RWC and the movable electrode. The ratio of d_0/A_0 does not depend on the frequency of the MEMC case vibrations.

In case of one or two collisions of the movable electrode with the stoppers on RWC the ratio d_0/A_0 is equal to $(0.5\pi - 1)$ and $(\pi/3 - \sqrt{3}/2)$, respectively. In general case, it is not possible to obtain analytical expressions for estimating the required value of the ratio d_0/A_0 for a given number of collisions. Figure 3 shows the dependence of the ratio d_0/A_0 on the number of collisions n of the movable electrode with the stoppers on the RWC, when the periodic motion of the movable electrode is realized.

It is obvious that for the double logarithmic scale this dependence is almost linear and with the error of less than 2% within the range of $1 < n < 20$ is well approximated by the following power function

$$d_0/A_0 = 0.596 \cdot n^{-\sqrt{3}}, \tag{4}$$

where n is the number of collisions between movable electrode and stoppers on the RWC.

According to Fig. 3 and Eq. (4), for increasing of the collisions number per one period of the case oscillation, keeping the amplitude constant, it is necessary to decrease the maximal value of the gap d_0 between the stoppers on the RWC and the movable electrode.

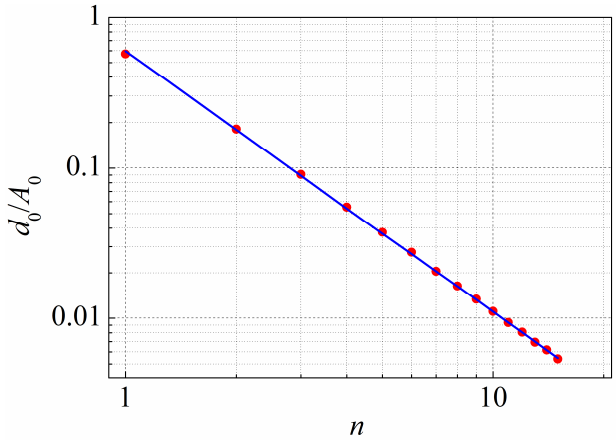

Fig. 3. The dependence of the ratio d_0/A_0 on the number of collisions n at which the periodic motion of the movable electrode is realized. Red circles – calculation using system of equations (3), solid line – calculation according to Eq. (4).

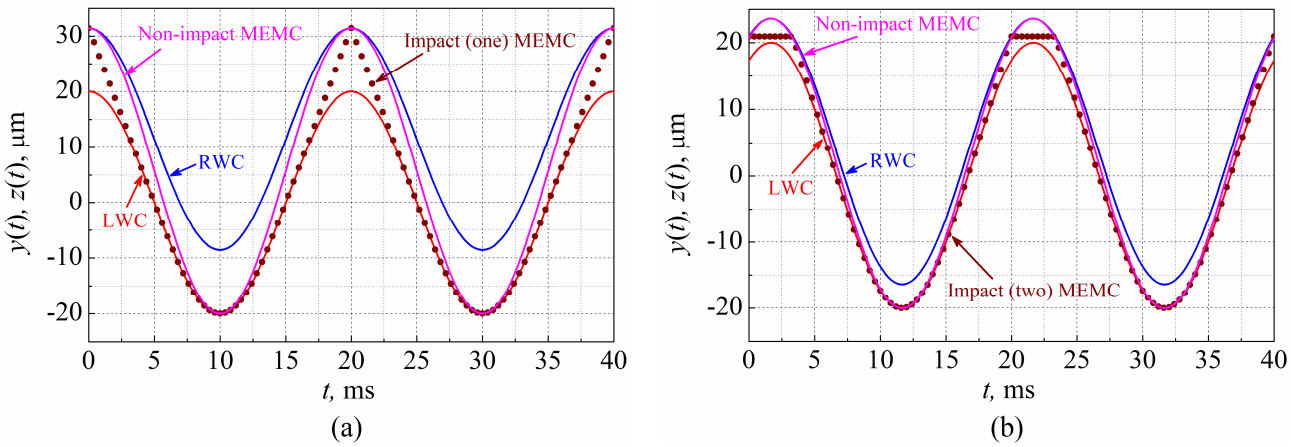

Fig. 4. Motion trajectories of the left (red lines) and right (blue lines) walls of the case, as well as the movable electrode for impact (circles) and non-impact (pink lines) MEMCs: (a) – one impact, (b) – two impacts.

Figure 4 shows the motion trajectories of the left and right walls of the case, as well as movable electrodes for impact MEMC, with one (a) and two (b) impacts during the period of the case vibration, and the corresponding non-impact MEMC calculated at $A_0 = 2 \cdot 10^{-5}$ m, $T = 0.02$ s and the corresponding ratios between d_0 and A_0.

Figures 5(a) and 5(b) show the time dependences of the change in the gap between the movable electrode and the stoppers on the RWC for the impact MEMC with one (a) and two (b) impacts during the oscillation period of the case and the corresponding non-impact MEMC, calculated with the same parameters as for Fig. 4.

Figures 5(c) and 5(d) show the time dependences of changes in the capacitance of the variable capacitor for the impact MEMC with one (c) and two (d) impacts during the oscillation period of the case and the corresponding non-impact MEMC, calculated with the same parameters as for Fig. 4, as well as with $\mu = 0.25$ and the area of the movable electrode $S = 6 \cdot 10^{-4}$ m^2.

The analysis of Fig. 5 and similar dependences for other MEMC with a large number of collisions shows that with a constant height of the stoppers the maximal capacitance modulation depth decreases when the number of collisions increases. But when the ratio d_0/A_0 and the height of the stoppers are proportionally reduced, the maximal capacitance modulation depth of MEMC remains unchanged. However if the collisions sequence number increases the capacitance modulation depth can be changed, as it can be seen from Fig. 6.

If the dependence of the capacitance of the variable capacitor is known then it is possible to analyze the operation of the microgenerator (e-VEH) as a whole.

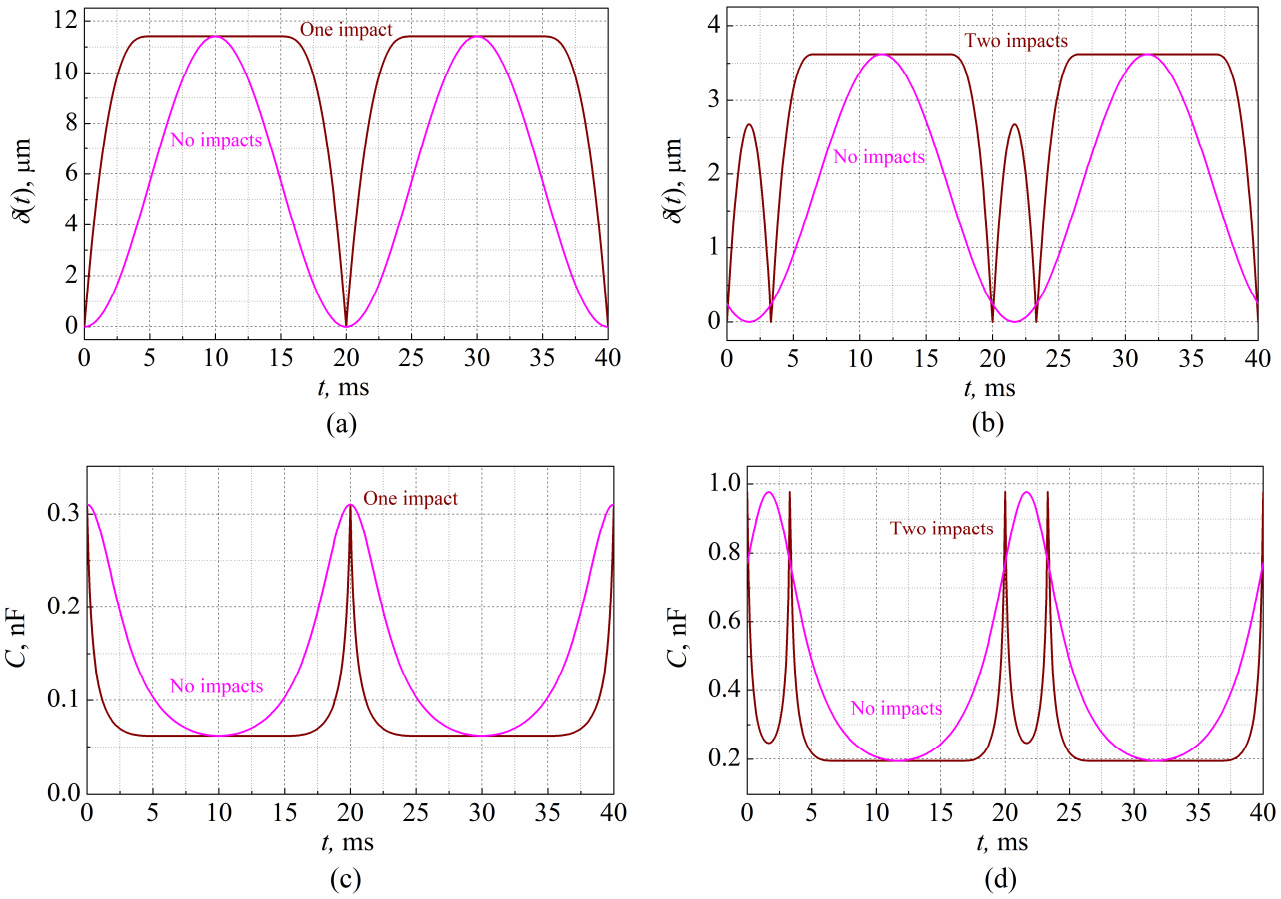

Fig. 5. Time dependences of changes in the gap between the movable electrode and the stoppers on the RWC (a, b) and changes of the capacitance (c, d) in the impact MEMC with one (a, c) and two (b, d) impacts. Brown lines are for impact MEMC and pink ones are for non-impact MEMC.

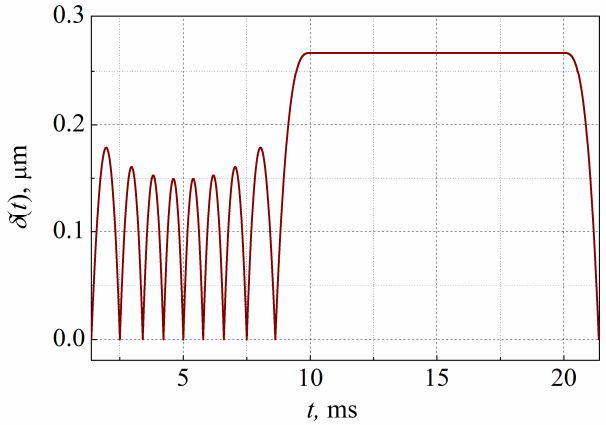

Fig. 6. Time dependence of changes in the gap between the movable electrode and the stoppers on the RWC in the impact MEMC (with nine collisions).

3. Microgenerator with Primary Source Charge Reduction

Let's consider the operation of the electrostatic microgenerator with a decrease of the primary source charge. Figure 7 shows the electric circuit of the microgenerator while includes the primary voltage source V_0, the switch Sw, the variable capacitor C, and the parallel connected load resistance R.

At the beginning when the capacitance of the variable capacitor reaches its maximal value (in our case when the movable electrode touches the stoppers on the RWC) the switch Sw is closed and the capacitor C is charged from the primary source V_0. After that, the charge of the capacitor becomes equal to $q_0 = C_{max}V_0$. Further, the movable electrode moves away from the stoppers on the RWC, the switch Sw is opened, the capacitance of the variable capacitor decreases, and then it is discharged through the load resistor R. Then the capacitance of the capacitor increases, but the capacitor continues to discharge. After the capacitance of the variable capacitor reaches its maximum again, the cycle repeats.

Figure 8 shows the time dependences of changes in the normalized charge (red lines) and voltage (blue lines) on the variable capacitor for the non-impact and impact (with two impacts during the period of case vibration) MEMC. The dependences were obtained with the same parameters as for Fig. 4 and $\mu = 0.25$, $V_0 = 5$ V, $R = 10^8$ Ω. For visibility, the time is counted from the moment of the first charge of the capacitor, when its capacity reaches the maximal value. The extended section of the capacitor discharge in Fig. 8(b) corresponds to the flat sections on the dependences of $\delta(t)$ and $C(t)$ in Figs. 5(b) and 5(d), respectively.

In order to determine whether a gain in the generated power and energy output is possible when using an impact MEMC or not, the dependences of the energy transferred to the load and taken from the primary power source over the period of case oscillations, as well as the rate of energy transfer (output power) versus the load resistance were calculated for microgenerators with different number of impacts n and the corresponding non-impact microgenerators. This correspondence means that the impact and non-impact MEMC have the same ratios d_0/A_0 and the stoppers height μd_0 depending on n. When analyzing the operation of the non-impact MEMC "n" shows which impact MEMC corresponds to the given non-impact one.

The calculations have shown that when the load resistance of both non-impact and impact microgenerators increases the energy transferred to the load during the period of vibrations of the case as well as the developed power at first increase and then decrease. That means there is some maximum of the power with an optimal load resistance R_{opt}. At the same time, the energy taken from the primary power source V_0 during the oscillation period of the case decreases monotonically when the load resistance increase. Also, when the load resistance increases the ratio between the energy transferred to the load and the energy taken from the primary voltage source V_0 increases all the time.

Figure 9 shows the dependences of the maximal power on the number of impacts during the period of the case vibration for impact (dashed lines) and non-impact (solid lines) e-VEHs calculated at $\mu = 1$, 0.5, 0.25, and 0.05. It is obvious from Fig. 9 that with the double logarithmic scale these dependences represent rising straight lines.

Comparing dependences shown in Fig. 9 it can be seen that when n increases the output power of the impact e-VEH grows faster than that for the non-impact one. Analysis shows that this is mainly due to the higher energy consumption of the primary source for the impact microgenerator than for the non-impact one. It should be also noted that as the value of n increases the value of R_{opt} for the impact microgenerator decreases faster than for the non-impact one (see Fig. 10). For $n \geq 2$ these dependences are well approximated by exponential functions with the form of $b_0 n^{b_1}$.

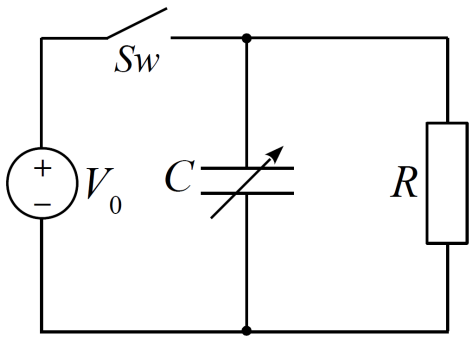

Fig. 7. The electric circuit of the microgenerator with a decrease of the primary source charge.

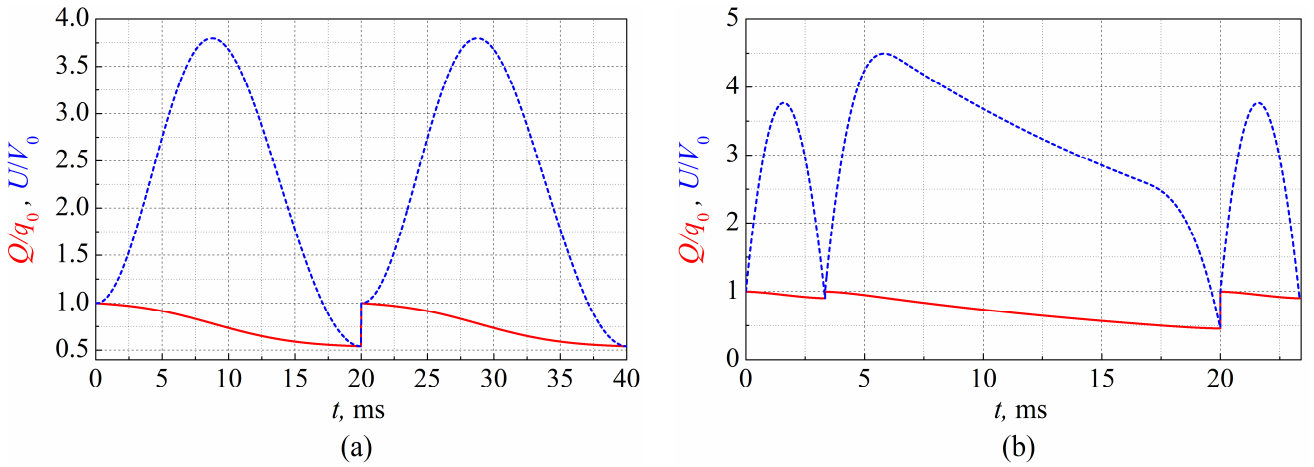

Fig. 8. Time dependences of changes in the charge (red lines) and voltage (blue lines) for non-impact (a) and impact (two impacts) (b) MEMC.

As a rule, when analyzing the operation of electrostatic microgenerators, it is usually adopted to determine the generated power only. However, an equally important parameter characterizing the operation of the microgenerator is the ratio Kw between the energy Wr transferred to the load and the energy Wv taken from the primary power source during the vibration period of the case.

Figure 11 shows the dependences of the ratio Kw for the impact and non-impact microgenerators on the number of impacts at R_{opt}. It is clear from Fig. 11 that this ratio for the impact e-VEH decreases when n increases. While for the non-impact microgenerator the value of the ratio Wr/Wv doesn't practically change.

Also a comparison of Kw for impact (triangles) and non-impact (circles) e-VEHs shows that: 1) the non-impact microgenerator converts the energy of the primary power source more efficiently than the corresponding impact one; 2) the use of both types of microgenerators with $\mu > 0.5$ is inexpedient for any n; 3) since the maximal capacitance modulation depth of the variable capacitor η at $\mu = 0.5$ is 3, then the use of MEMC with $\eta \le 3$ in such e-VEHs is also inexpedient.

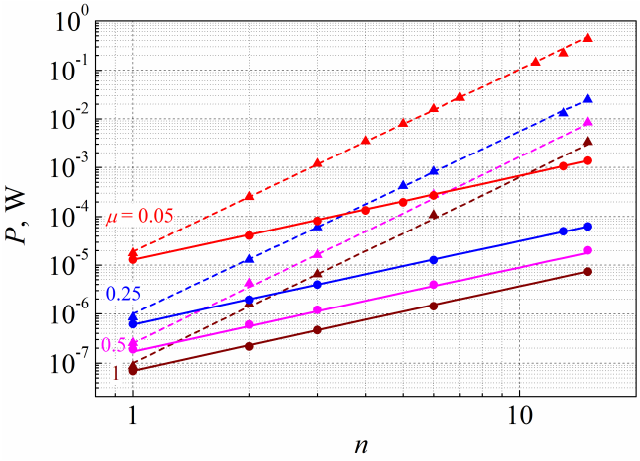

Fig. 9. The dependences of the maximum power on the number of collisions n for impact (dashed lines) and non-impact (solid lines) e-VEHs.

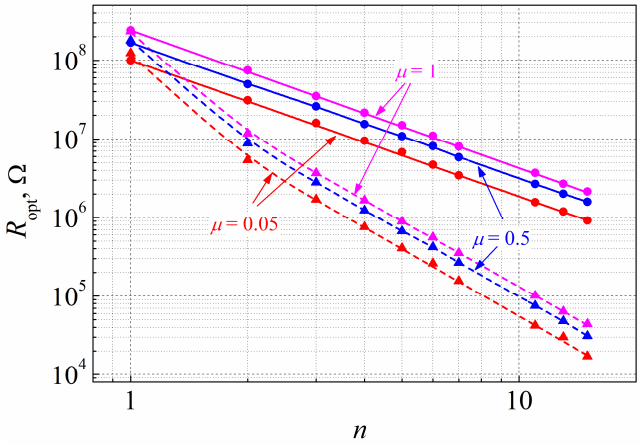

Fig. 10. The dependences of the optimal load resistance R_{opt} on the number of collisions n for impact (dashed lines) and non-impact (solid lines) e-VEHs.

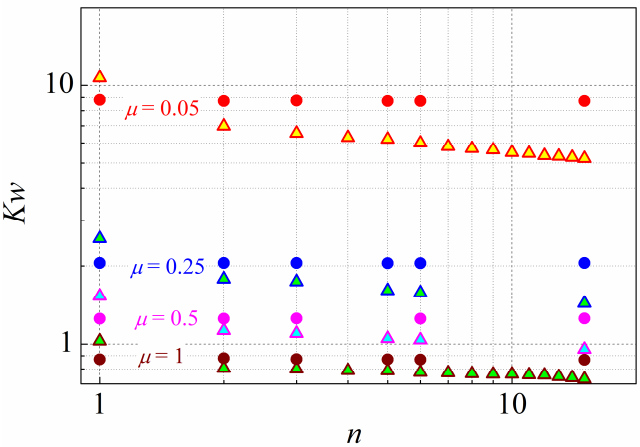

Fig. 11. The dependences of the ratio Kw for the impact (triangles) and non-impact (circles) e-VEHs on the number of impacts at R_{opt}.

Because in practice, it is rather difficult to create a MEMC with $\eta \geq 5$, which corresponds to $\mu \leq 0.25$, then it is problematic to create an e-VEH of this type with $Kw > 2$. Thus, the period between servicing of the primary power source (replacement or charging) in an autonomous WSN when using an e-VEH of this type will actually increase by no more than two times.

The problem of increasing the ratio Kw between the energy Wr transferred to the load and the energy Wv taken from the primary power source can be solved using the e-VEHs where one of the electrodes has an electret layer [37-39] or the capacitor electrodes are made of materials with different work functions [40-42], as well as in e-VEHs with the primary source charge conservation, which will be discussed below.

4. Microgenerator with Primary Source Charge Conservation

Let's consider the operation of the electrostatic e-VEH with the charge conservation of the primary source. Figure 12 shows the electric circuit of the microgenerator which comprises the primary voltage source V_0, the variable capacitor (MEMC) C, and the series-connected load resistance R.

During the operation of this microgenerator when the capacitance of the variable capacitor increases (in our case, when the movable electrode moves to the RWC), the capacitor C is charged from the primary voltage source V_0. At the moment of contact between the movable electrode and the stoppers on the RWC the capacitance of the capacitor reaches its maximum. Then the movable electrode moves away from the RWC, the capacitance of the capacitor decreases and it is discharged through the load R. Further, the capacitance of the capacitor increases again. After the capacitance of the capacitor reaches its maximum again, the cycle repeats. In this case, after the end of the transient process, the change of the primary voltage source charge during the conversion cycle is equal to zero.

Figure 13 shows the dependences of the normalized charge (red line), voltage (blue line) and capacitance (green line) of the variable capacitor for non-impact (a) and impact (two impacts) (b) microgenerators calculated at the same parameters as for Fig. 8, but at $R = 5 \cdot 10^6$ Ω. The time is counted off from the first variable capacitor charge, when its capacitance is maximal. The extended section of the capacitor discharge in Fig. 13(b) corresponds to the flat sections on the dependences of $\delta(t)$ and $C(t)$ in Figs. 5(b) and 5(d), respectively.

It is clear from Fig. 13 that after transient processes for both cases (non-impact and impact) steady-state processes appear, and the maximal charge across the capacitor is reached not when the capacitance is maximal, but when it starts to decrease.

Calculations have shown that in the steady state when the load resistance increases, for both non-impact and impact e-VEHs the energy delivered to the load during the period of vibrations of the case as well as the developed output power first increase and then decrease. That means there is an optimal load resistance R_{opt}.

Figure 14 shows the dependences of the maximal power on the number of impacts during the period of the case vibration for impact (dashed lines) and non-impact (solid lines) e-VEHs calculated at $\mu = 1$, 0.5, 0.25, and 0.05 and R_{opt}. It is clear that with the double logarithmic scale these dependences correspond to rising straight lines, similar to the dependences shown in Fig. 9.

Comparing dependences shown in Fig. 14 one can see that when n increases the output power of the impact e-VEH grows faster than that of the non-impact one. Also for $n > 2$ the power of the impact microgenerator becomes greater than that of the non-impact one. It should be noted that for the impact microgenerator the value of R_{opt} decreases faster than for the non-impact one when the value of n increases (see Fig. 15).

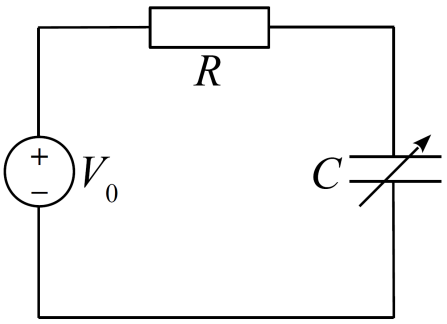

Fig. 12. The electric circuit of the microgenerator with the primary source charge conservation.

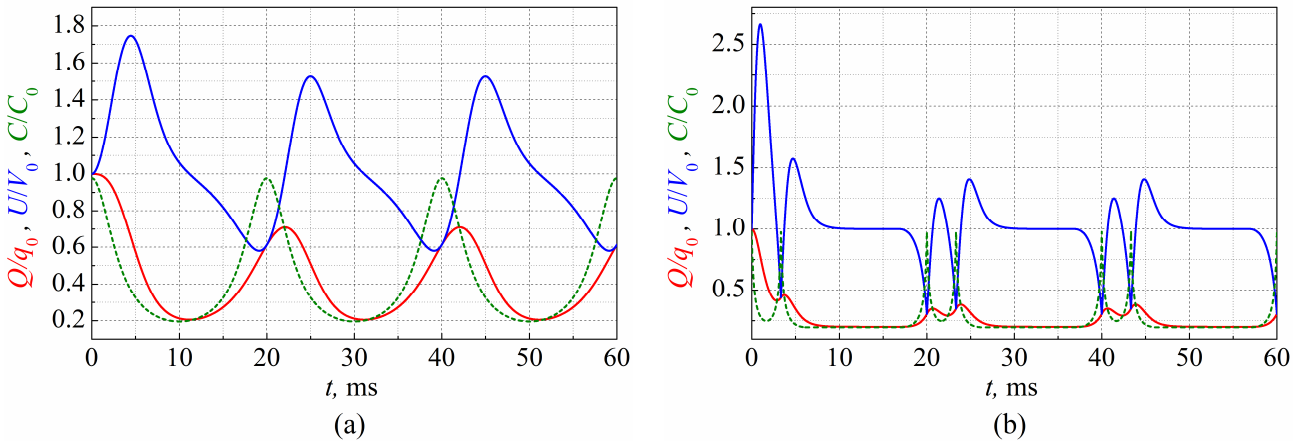

Fig. 13. The dependences of the normalized charge (red), voltage (blue) and capacitance (green) of the variable capacitor for non-impact (a) and impact (two impacts) (b) microgenerators.

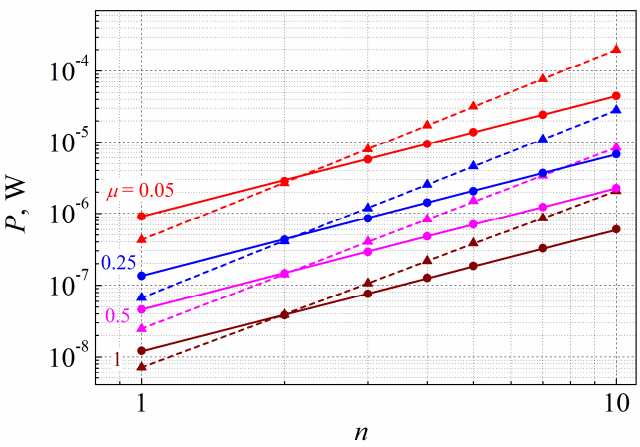

Fig. 14. The dependences of the maximum power on the number of collisions n for impact (dashed lines) and non-impact (solid lines) e-VEHs.

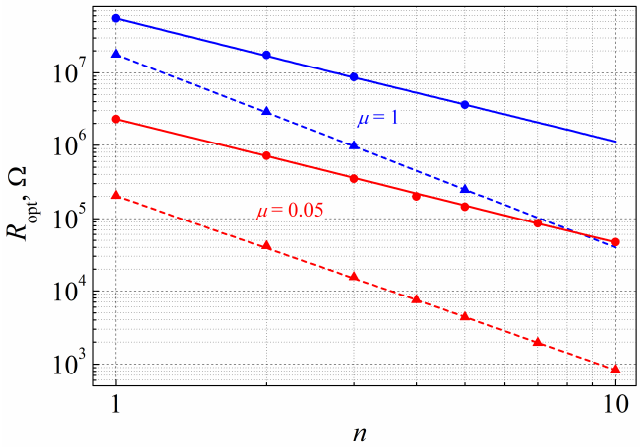

Fig. 15. The dependences of the optimal load resistance R_{opt} on the number of collisions n for impact (dashed lines) and non-impact (solid lines) e-VEHs.

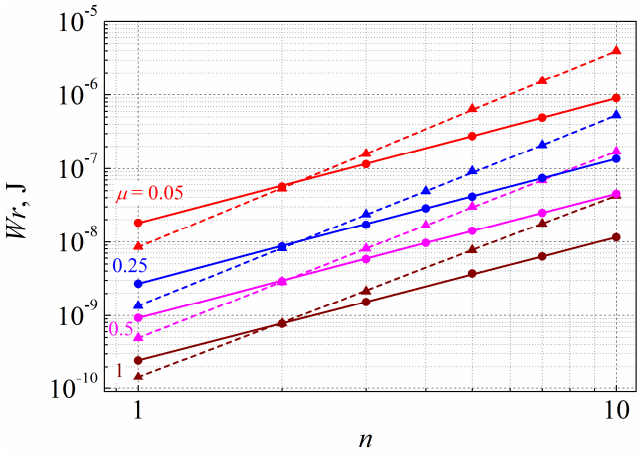

Fig. 16. The dependences of the energy Wr transferred to the load on the number of impacts n calculated at R_{opt} for the impact (dashed lines) and non-impact (solid lines) e-VEHs.

Figure 16 shows the dependences of the energy Wr transferred to the load during the period of the case vibration for impact and non-impact e-VEHs on the number of collisions n, calculated at R_{opt}. It is evident that Wr increases as the value of n increases, and the dependences themselves are well approximated by exponential functions with the form of $b_0 n^{b1}$, including points at $n = 1$. It is also clear from Fig. 16 that when $n > 2$ the energy transferred to the load is higher for the impact e-VEH than for the non-impact one.

5. Results Discussion

The analysis shows that only at certain ratios between the maximal interelectrode gap and the amplitude of the case vibrations, the motion of the movable electrode will be periodic.

It has been found that the dependence of this ratio on the number of collisions n during the period of the case vibrations in the interval of $1 < n < 20$ is well approximated by the following exponential function

$$d_0/A_0 = 0.596 \cdot n^{-\sqrt{3}}.$$

With a constant height of the stoppers, the maximal capacitance modulation depth decreases as the number of collisions increases. If the ratio of d_0/A_0 is reduced proportionally along with the height of the stoppers, then the maximal capacitance modulation depth of the MEMC will remain constant.

Analysis of the e-VEH operation with the primary source charge reduction showed the following:

– when the load resistance increases for both impact and non-impact e-VEHs the energy transferred to the load during the period of the case vibrations as well as the developed output power first increase and then decrease. At the same time, the energy taken from the primary voltage source during the vibration period of the case decreases monotonically. Also, as the load resistance increases the ratio between the energy Wr transferred to the load and the energy Wv taken from the primary voltage source increases all the time;

– when the value of n increases the power of the impact e-VEH grows faster than that of the non-impact e-VEH. However, this is mainly due to the greater energy consumption of the primary voltage source for the impact e-VEH relative to the non-impact one;

– when the value of n increases the optimal load resistance R_{opt} for the impact e-VEH decreases faster than for the non-impact one, and for $n \geq 2$ these dependences are well described by exponential functions with the form of $b_0 n^{b1}$;

– when the value of n increases the ratio of Wr/Wv for the impact e-VEH at R_{opt} monotonically decreases. While for the non-impact e-VEH this ratio practically does not change;

– the non-impact e-VEH converts the energy of the primary power source more efficiently than the corresponding impact e-VEH;

– the use of the both types of the e-VEHs with $\mu > 0.5$ and with $\eta \leq 3$ is useless for any n.

Since in practice it is rather difficult to make the MEMC with $\eta \geq 5$, then the creation of this type of e-VEHs with $Kw > 2$ is problematic. Thus, the period between maintenance of the primary power source (replacement or charging) in WSN nodes with such e-VEHs can be increased by no more than two times. It should be also noted that a unipolar voltage is generated by this type of e-VEHs.

In turn, the analysis of the e-VEH operation with the primary source charge conservation showed the following:

– when the value of n increases the output power of the impact e-VEH grows faster than for the non-impact one, and for $n > 2$ the power of the impact e-VEH becomes greater than that of the non-impact one;

– the dependences of the maximal power on the number of impacts during the period of the case vibration for impact and non-impact e-VEHs are well described by exponential functions;

– when the value of n increases the optimal load resistance R_{opt} for the impact e-VEH decreases faster than for the non-impact one;

– when the value of n increases the energy Wr transferred to the load during the case vibration period for impact and non-impact e-VEHs increases, and the dependences themselves are well approximated by exponential functions including the points at $n = 1$. Also for $n > 2$ the energy transferred to the load for the impact e-VEH becomes higher than that for the non-impact one.

It should be noted that the e-VEH of this type converts the mechanical vibration energy less efficiently than the e-VEH with the primary source charge reduction. In addition, it generates alternating voltage. However, since the charge is not taken from the primary voltage source on average during the oscillation period, then theoretically the period between maintenance of the primary power source may be not limited when using this type of e-VEH.

When analyzing the operation of the e-VEHs, it was assumed that the electrical and mechanical forces are insignificant in comparison with the external driving force, and the movable electrode moves according to the trajectories described in Section 2. The MEMC charge occurs when the capacity is at its maximum, and the discharge occurs when it is at the minimum.

Taking into account the finite stiffness of the elastic suspensions, solution of Eq. (1) can take the form of

$$\delta = d_0 - \left\{\cos\left(\frac{\omega}{\gamma}t\right)Y_0 + \frac{\gamma}{\omega}\sin\left(\frac{\omega}{\gamma}t\right)v_0 + A_0\frac{\gamma^2}{\gamma^2-1}\left[\gamma\sin\left(\frac{\omega}{\gamma}t\right) - \sin(\omega t)\right]\right\}, \quad (5)$$

where $\gamma = \omega/\omega_0$, and ω_0 is the natural vibration frequency of the vibrating system.

As in the case of zero stiffness, in order for the behavior of the system with finite stiffness of elastic suspensions to become periodic, it is necessary to take into account that $v_1(t)$ and $V_1(t)$ have to be equal to $v_1(t+T)$ and $V_1(t+T)$, respectively, when compiling a system of equations describing the e-VEH behavior.

During designing and simulation of the both impact and non-impact MEMC it is necessary to have an idea about the ratio between the converter parameters and the external driving force, which is necessary to implement impacts in the system. It can be shown using Eq. (5) that in order to have at least one impact between the movable electrode and RWC stoppers during the first vibration period, for a given γ, the interelectrode gap d_0 cannot exceed the following value

$$d_{0,cr} = A_0\frac{\gamma^2}{\gamma^2-1}\left[\gamma\sin\left(\frac{2\pi}{1+\gamma}\right) - \sin\left(\frac{2\pi\gamma}{1+\gamma}\right)\right],$$

where the contact itself will occur at the moment of

$$t_{cr} = \frac{1}{\omega}\frac{2\pi\gamma}{1+\gamma},$$

and the periodic mode with one contact against the RWC stoppers will occur when

$$\frac{d_0}{A_0} = \frac{\gamma^2}{\gamma^2-1}\left[\gamma\sin\left(\frac{\pi}{2\gamma}\right) - 1\right].$$

These expressions enable to evaluate whether the presence of impacts in a given MEMC is possible or not, as well as what parameters and how must be changed for impacts appearance or disappearance.

Moreover, using Eqs. (2) and (5) one can obtain equation systems describing the behavior of the MEMC with an arbitrary number of impacts during the case vibration period. For example, for a MEMC with four impacts during the period such a system of equations determining the parameters of the e-VEH takes the following form

$$\frac{d_0}{A_0}=\frac{\omega^2}{\omega^2-\omega_0^2}\left[\frac{\omega}{\omega_0}\sin(\omega_0 t_1)-\sin(\omega t_1)\right],$$

$$\frac{d_0}{A_0}=\frac{1}{1-\cos(\omega_0\Delta t)}\left\{\cos(\omega_0\Delta t)\sin(\omega t_1)+\frac{\omega^2}{\omega^2-\omega_0^2}\left[\frac{\omega}{\omega_0}\sin(\omega_0\Delta t)\cdot\left[1-\cos(\omega_0 t_1)+\frac{2\omega^2-\omega_0^2}{\omega^2}\cos(\omega t_1)\right]-\sin(\omega\Delta t)\right]-\sin(\omega t_2)\right\},$$

$$\frac{d_0}{A_0}=\frac{1}{\omega_0\sin(\omega_0\Delta t)}\left\{-\omega_0\sin(\omega_0\Delta t)\sin(\omega t_1)+\frac{\omega^3}{\omega^2-\omega_0^2}\left[\cos(\omega_0\Delta t)\cdot\left[1-\cos(\omega_0 t_1)+\frac{2\omega^2-\omega_0^2}{\omega^2}\cos(\omega t_1)\right]-\cos(\omega\Delta t)\right]-2\omega\cos(\omega t_2)\right\},$$

where $\Delta t = t_2 - t_1$. The expressions obtained show that when the finite stiffness of the suspensions is taken into account, the ratio d_0/A_0 at which periodic impacts are possible now depends on the frequency of the driving force ω and the value of ω/ω_0. The analysis of the natural oscillations of the MEMC and the estimates made using these expressions and Eq. (3) tend to each other. Thus, the estimates made by means of Eq. (3) can be used both independently and as initial approximations when using equations that take into account the value of γ. These estimates should be considered as the maximum possible.

At the same time, using the analysis based on Eq. (5), it is possible to refine the necessary parameters of the system. For example, for $\gamma = 2$ and the vibration frequency of the system case of 50 Hz, the dependence of the ratio d_0/A_0, at which the periodic motion of the movable electrode will take place, on the number of impacts between the movable electrode and the stoppers on the RWC is defined as

$$d_0/A_0 = 0.57\cdot n^{-\sqrt{2.3}} + 0.1\cdot n^{0.01}.$$

That is as the value of γ decreases the dependence of the ratio d_0/A_0 on the impact number is significantly weakened. If necessary, the presence of losses (mechanical and electrical) can be also taken into account. For example, calculations show that if the mechanical loss factor $B < 0.01$ kg/s, then these losses don't practically affect on the analysis results.

In general, the analysis performed and the approach developed make it possible to significantly limit the range of searching for the necessary system parameters at the preliminary design stage and to reduce the design time.

6. Conclusions

The microgenerator (e-VEH) operation in the periodic impact mode is analyzed on the basis of circuits with serial and parallel connection of the load. The necessary condition for the implementation of the impact mode of MEMC operation has been obtained. The dependences of the average generated power of the impact e-VEH (microgenerators) on the number of impacts and the load resistivity are calculated. The efficiency of the impact and corresponding non-impact e-VEHs has been compared. It has been established that when using the impact e-VEH the gain of the output power by 1-2 orders of magnitude along with a significant decrease of the optimal load is possible in comparison with the use of the corresponding non-impact e-VEH.

Author Contributions

V. P. Dragunov planned the scheme, initiated the project, and suggested the mathematical model; D. I. Ostertak developed the mathematical model and analyzed the results; D. E. Kiselev carried out the calculations; E. V. Dragunova presented the literature survey. The manuscript was written through the contribution of all authors. All authors discussed the results, reviewed, and approved the final version of the manuscript.

Acknowledgements

Not applicable.

Conflict of Interest

The authors declared no potential conflicts of interest concerning the research, authorship, and publication of this article.

Funding

The reported study was supported by the Ministry of Science and Higher Education of the Russian Federation (project FSUN-2020-0004).

Data Availability Statements

The datasets generated and/or analyzed during the current study are available from the corresponding author on reasonable request.

Nomenclature

A_0	Amplitude of the case oscillations [m]	t_1	Time of the first impact [s]
B	Damping force coefficient [kg/s]	t_2	Time of the second impact [s]
b_0, b_1	Approximating coefficients	t_3	Time of the third impact [s]

C	Capacitance of the variable capacitor [F]	t_4	Time of the fourth impact [s]
C_{max}	Maximal value of capacitance C [F]	V_0	Primary source voltage [V]
C_{min}	Minimal value of capacitance C [F]	V_1	Velocity of the movable electrode after the impact [m/s]
d_0	Maximal gap between the stoppers on the right wall case and the movable electrode [m]	V_2	Velocity of the case after the impact [m/s]
e	Velocity recovery coefficient	Wr	Energy transferred to the load during the vibration period of the case [J]
F_e	Electrostatic force between the stoppers on the RWC and the movable electrode [N]	Wv	Energy taken from the primary power source during the vibration period of the case [J]
k	Spring elements stiffness [N/m]	x	Gap between the stoppers on the LWC and the movable electrode [m]
Kw	Ratio between the energy transferred to the load and the energy taken from the primary power source during the vibration period of the case	$y(t)$	Law of the converter case motion [m]
M_1	Movable electrode mass [kg]	Y_0	Initial displacement of the movable electrode calculated after each collision [m]
M_2	Case mass [kg]	$z(t)$	Law of movable electrode motion [m]
n	Number of impacts	γ	Ratio between the angular frequency of the case oscillations and natural vibration frequency of the vibrating system
q_0	Charge taken from the primary power source [C]	δ	Gap between the stoppers on the right wall case and the movable electrode [m]
R	Load resistance [Ω]	η	Capacitance modulation depth of the variable capacitor
R_{opt}	Optimal load resistance [Ω]	μ	Coefficient of proportionality defining the stopper height
S	Area of the movable electrode [m^2]	υ_0	Initial velocity of the movable electrode calculated after each collision [m/s]
Sw	Circuit switch	υ_1	Velocity of the movable electrode before the impact [m/s]
T	Period of the case oscillation [s]	υ_2	Velocity of the case before the impact [m/s]
t	Time [s]	ω	Angular frequency of the case oscillations [s^{-1}]
t_0	Initial moment of time [s]	ω_0	Natural vibration frequency of the vibrating system [s^{-1}]

References

[1] Heydarishahreza, N., Ebadollahi, S., Vahidnia, R., Dian, F. J., Wireless Sensor Networks Fundamentals: A Review, *2020 11th IEEE Annual Information Technology, Electronics and Mobile Communication Conference (IEMCON)*, Vancouver, Canada, 0001–0007, 2020.
[2] Khan, S., Pathan, A.-S., Alrajeh, N., *Wireless Sensor Networks: current status and future trends*, CRC Press, Boca Raton, 2016.
[3] Harb, A., Energy harvesting: State-of-the-art, *Renewable Energy*, 36, 2011, 2641–2654.
[4] Vullers, R. J. M., van Schaijk, R., Doms, I., Van Hoof, C., Mertens, R., Micropower energy harvesting, *Solid-State Electronics*, 53, 2009, 684–693.
[5] Wei, C., Jing, X., A comprehensive review on vibration energy harvesting: Modelling and realization, *Renewable and Sustainable Energy Reviews*, 74, 2017, 1–18.
[6] Khan, F. U., Review of non-resonant vibration based energy harvesters for wireless sensor nodes, *Journal of Renewable and Sustainable Energy*, 8, 2016, 044702.
[7] Mitcheson, P. D., Yeatman, E. M., Rao, G. K., Holmes, A. S., Green, T. C., Energy Harvesting From Human and Machine Motion for Wireless Electronic Devices, *Proceedings of the IEEE*, 96 (9), 2008, 1457–1486.
[8] Cai, M., Yang, Z., Cao, J., Liao, W.-H., Recent Advances in Human Motion Excited Energy Harvesting Systems for Wearables, *Energy Technology,* 8, 2020, 2000533.
[9] Yanazawa, H., Homma, K., Growing market of MEMS and technology development in process and tools specialized to MEMS, *2017 IEEE Electron Devices Technology and Manufacturing Conference (EDTM),* Toyama, Japan, 143–144, 2017.
[10] Mishra, M. K., Dubey, V., Mishra, P. M., Khan, I., MEMS Technology: A Review, *Journal of Engineering Research and Reports*, 4 (1), 2019, 46001.
[11] Wang, G., Liao, W.-H., Yang, B., Wang, X., Xu, W., Li, X., Dynamic and Energetic Characteristics of a Bistable Piezoelectric Vibration Energy Harvester with an Elastic Magnifier, *Mechanical Systems and Signal Processing*, 105, 2018, 427–446.
[12] Yin, Z., Gao, S., Jin, L., Sun, Y., Wu, Q., Zhang, X., Guo, S., A Dual Impact Driven Frequency Up-Conversion Piezoelectric Energy Harvester for Ultralow-Frequency and Wide-Bandwidth Operation, *Sensors and Actuators A: Physical,* 331, 2021, 112961.
[13] Woo, M. S., Ahn, J. H., Eom, J. H., Hwang, W. S., Kim, J. H., Yang, C. H., Song, G. J., Hong, S. D., Jhun, J. P., Sung, T. H., Study on Increasing Output Current of Piezoelectric Energy Harvester by Fabrication of Multilayer Thick Film, *Sensors and Actuators A: Physical,* 269, 2018, 524–534.
[14] Khan, F. U., Iqbal, M., Electromagnetic Bridge Energy Harvester Utilizing Bridge's Vibrations and Ambient Wind for Wireless Sensor Node Application, *Journal of Sensors,* 2018, 3849683.
[15] Li, Y., Zhou, C., Cao, Q., Wang, X., Qiao, D., Tao, K., Electromagnetic Vibration Energy Harvester with Tunable Resonance Frequency Based on Stress Modulation of Flexible Springs, *Micromachines,* 12(9), 2021, 1130.
[16] Gunn, B., Alevras, P., Flint, J. A., Fu, H., Rothberg, S. J., Theodossiades, S., A Self-Tuned Rotational Vibration Energy Harvester for Self-Powered Wireless Sensing in Powertrains, *Applied Energy*, 302, 2021, 117479.
[17] Khan, F. U., Qadir, M. U., State-of-the-Art in Vibration-Based Electrostatic Energy Harvesting, *Journal of Micromechanics and Microengineering,* 26 (10), 2016, 103001.
[18] Dragunov, V. P., Ostertak, D. I., Pelmenev, K. G., Sinitskiy, R. E., Dragunova, E. V., Electrostatic Vibrational Energy Converter with Two Variable Capacitors, *Sensors and Actuators A: Physical*, 318, 2021, 112501.
[19] Guo, X., Zhang, Y., Fan, K., Lee, C., Wang, F., A Comprehensive Study of Non-Linear Air Damping and "Pull-in" Effects on the Electrostatic Energy Harvesters, *Energy Conversion and Management*, 203, 2020, 112264.
[20] Dragunov, V. P., Ostertak, D. I., Sinitskiy, R. E., New Modifications of a Bennet Doubler Circuit-Based Electrostatic Vibrational Energy Harvester, *Sensors and Actuators A: Physical*, 302, 2020, 111812.
[21] Xia, K., Chi, Y., Fu, J., Zhu, Z., Zhang, H., Du, C., Xu, Z., A Triboelectric Nanogenerator Based on Cosmetic Fixing Powder for Mechanical Energy Harvesting, *Microsystems & Nanoengineering*, 5 (1), 2019, 26.
[22] Zhang, D., Shi, J., Si, Y., Li, T., Multi-Grating Triboelectric Nanogenerator for Harvesting Low-Frequency Ocean Wave Energy, *Nano Energy*, 61, 2019,

132–140.
[23] Luo, A., Zhang, Y., Guo, X., Lu, Y., Lee, C., Wang, F., Optimization of MEMS Vibration Energy Harvester with Perforated Electrode, *Journal of Microelectromechanical Systems*, 30 (2), 2021, 299–308.
[24] Tao, K., Yi, H., Yang, Y., Tang, L., Yang, Z., Wu, J., Chang, H., Yuan, W., Miura-Origami-Inspired Electret/Triboelectric Power Generator for Wearable Energy Harvesting with Water-Proof Capability, *Microsystems & Nanoengineering*, 6 (1), 2020, 56.
[25] Luo, A., Xu, Y., Zhang, Y., Zhang, M., Zhang, X., Lu, Y., Wang, F., Spray-Coated Electret Materials with Enhanced Stability in a Harsh Environment for an MEMS Energy Harvesting Device, *Microsystems & Nanoengineering*, 7 (1), 2021, 15.
[26] Tao, K., Chen, Z., Yi, H., Zhang, R., Shen, Q., Wu, J., Tang, L., Fan, K., Fu, Y., Miao, J., Yuan, W., Hierarchical Honeycomb-Structured Electret/Triboelectric Nanogenerator for Biomechanical and Morphing Wing Energy Harvesting, *Nano-Micro Letters*, 13 (1), 2021, 123.
[27] Fan, K., Wei, D., Zhang, Y., Wang, P., Tao, K., Yang, R., A Whirligig-Inspired Intermittent-Contact Triboelectric Nanogenerator for Efficient Low-Frequency Vibration Energy Harvesting, *Nano Energy*, 90, 2021, 106576.
[28] Tao, K., Zhao, Z., Yang, Y., Wu, J., Li, Y., Fan, K., Fu, Y., Chang, H., Yuan, W., Development of Bipolar-Charged Electret Rotatory Power Generator and Application in Self-Powered Intelligent Thrust Bearing, *Nano Energy*, 90, 2021, 106491.
[29] Le, C. P., Halvorsen, E., Søråsen, O., Yeatman, E. M., Microscale Electrostatic Energy Harvester Using Internal Impacts, *Journal of Intelligent Material Systems and Structures*, 23 (13), 2012, 1409–1421.
[30] Phu, C., Halvorsen, E., *Microscale Energy Harvesters with Nonlinearities Due to Internal Impacts*, *Small-Scale Energy Harvesting*, InTech, London, 2012.
[31] Basset, P., Galayko, D., Cottone, F., Guillemet, R., Blokhina, E., Marty, F., Bourouina, T., Electrostatic Vibration Energy Harvester with Combined Effect of Electrical Nonlinearities and Mechanical Impact, *Journal of Micromechanics and Microengineering*, 24 (3), 2014, 035001.
[32] Yuksek, N. S., Zhu, J., Feng, Z. C., Almasri, M., MEMS Capacitors with Dual Cavity for Power Harvesting, *SPIE Defense, Security, and Sensing*, Baltimore, USA, 83770P, 2012.
[33] Lin, J., Zhu, J., Feng, Z., Almasri, M., Two-Cavity MEMS Capacitive Power Scavenger, *SPIE Defense, Security, and Sensing*, Baltimore, USA, 83770O, 2012.
[34] Baginsky, I. L., Kostsov, E. G., Sokolov, A. A., New Approach to the Development of Impact-Type Electrostatic Microgenerators, *Optoelectronics, Instrumentation and Data Processing*, 51 (3), 2015, 310–320.
[35] Li, S., Peng, Z., Zhang, A., Wang, F., Dual resonant structure for energy harvesting from random vibration sources at low frequency, *AIP Advances*, 6 (1), 2016, 015019.
[36] Li, S., Crovetto, A., Peng, Z., Zhang, A., Hansen, O., Wang, M., Li, X., Wang, F., Bi-resonant structure with piezoelectric PVDF films for energy harvesting from random vibration sources at low frequency, *Sensors and Actuators A: Physical*, 247, 2016, 547–554.
[37] Chen, G., Tang, L., Yang, Z., Tao, K., Yu, Z., An Electret-based Thermoacoustic-electrostatic Power Generator, *International Journal of Energy Research*, 44 (3), 2020, 2298–2305.
[38] Zhang, Y., Guo, X., Liu, Z., Luo, A., Wang, F., Two Mechanical Tuning Schemes to Improve the Bandwidth of Electret-Based Electrostatic Energy Harvester, *2018 IEEE/ASME International Conference on Advanced Intelligent Mechatronics (AIM)*, Auckland, New Zealand, 375–380, 2018.
[39] Zhang, Y., Wang, T., Luo, A., Hu, Y., Li, X., Wang, F., Micro Electrostatic Energy Harvester with Both Broad Bandwidth and High Normalized Power Density, *Applied Energy*, 212, 2018, 362–371.
[40] Varpula, A., Laakso, S. J., Havia, T., Kyynäräinen, J., Prunnila, M., Harvesting Vibrational Energy Using Material Work Functions, *Scientific Reports*, 4 (1), 2015, 6799.
[41] Ostertak, D. I., Sinitskiy, R. E., Dragunov, V. P., Operation Features of Electrostatic Vibrational Energy Harvester Based on Contact Potential Difference, *Journal of Physics: Conference Series*, 1353, 2019, 012097.
[42] Kuehne, I., Frey, A., Marinkovic, D., Eckstein, G., Seidel, H., Power MEMS—A Capacitive Vibration-to-Electrical Energy Converter with Built-in Voltage, *Sensors and Actuators A: Physical*, 142 (1), 2008, 263–269.

ORCID iD

Valery P. Dragunov https://orcid.org/0000-0002-7088-5727
Dmitriy I. Ostertak https://orcid.org/0000-0003-2903-0732
Dmitry E. Kiselev https://orcid.org/0000-0001-7693-1053
Evgeniya V. Dragunova https://orcid.org/0000-0002-0677-9735

How to cite this article: Dragunov V.P., Ostertak D.I., Kiselev D.E., Dragunova E.V. Impact-enhanced Electrostatic Vibration Energy Harvester, *J. Appl. Comput. Mech.*, 8(2), 2022, 671–683. https://doi.org/10.22055/JACM.2021.38781.3312